Does mineralization and pH control the distribution of ammonia-oxidizing archaea in temperate forest soils?

By Jennifer Wen

Thesis submitted in partial fulfillment of the requirements
for the degree of Master of Science
(School for Environment and Sustainability)
at the University of Michigan
April 2022

Thesis Committee:
Professor Donald R. Zak, Chair
Professor Aimée Classen

Abstract

Ammonia-oxidizing archaea (AOA) are a primary contributor to nitrification – a key process in nutrient cycling that influences the concentration of nitrate in forest ecosystems. This study addressed (1) how AOA community composition changes across upland forest stands in Manistee National Forest and (2) how environmental factors such as pH and net N mineralization may be associated with AOA distribution. From collected soil samples, *amoA* (a functional gene involved in ammonia oxidation) was amplified and sequenced to detect AOA. Sequences were classified based on the known taxonomy of AOA, and the relative abundances of AOA taxa were compared between stands and along changes in pH and mineralization.

Results of PERMANOVA and Mantel tests show that both pH and net N mineralization are significantly associated with AOA distribution ($p < 0.05$). Moreover, pH is a stronger predictor of AOA distribution than mineralization, contributing to up to 23% of variations in community composition, while mineralization contributes 8%. Phylogenetic analyses revealed that two AOA lineages are represented in the stands: *Nitrososphaeales* and *Ca.* Nitrosotaleales. Titan analyses revealed that within these lineages, specific taxa can be negatively correlated or positively correlated with pH and mineralization. Furthermore, the relative abundance of these lineages and their clades are markedly different across stands.

These results show that AOA communities can be very distinct within similar ecosystem types. Furthermore, AOA taxa do not share a single directional response to pH or net mineralization, emphasizing the diversity of AOA and their interactions with the environment. In this study, we were able to contribute to an understanding of how a gradient of environmental factors is associated with the distribution of nitrifying microorganisms, and we recommend to incorporating AOB abundances into future research on the composition and relative contributions of ammonia-oxidizing organisms to nitrification

Acknowledgements

I would like to sincerely thank my advisor, professors, colleagues, friends, family, and SEAS for their support throughout my Master's program leading up to the completion of this thesis. First and foremost, my deepest gratitude to my advisor and thesis chair, Dr. Donald Zak, for continually providing guidance, encouragement, and inspiration as well as introducing me to the wonderful world of soil microecology. Your insights have made me a better ecologist and person. I am also incredibly grateful for Rima Upchurch for helping me with my project every step of the way, from the lab work, the bioinformatics, and the statistics. You made three daunting fields much more manageable, and I could neither have completed my thesis nor learned as much as I did without your help. I also thank my colleague William Argiroff for providing the field samples and data that form the basis of my research, and Dr. Aimée Classen for your insights and help with my manuscript. I am grateful for SEAS and Peter and Carolyn Mertz for their financial assistance, and the support of the University of Michigan Medical School Microbiome Core. Lastly, I thank my friends, family, and partner for their unconditional support, even in the hardest of times over these short two years.

Table of Contents

1. Introduction

Nitrification is a prevalent and important process in the nitrogen cycle that researchers thought was controlled solely by ammonia-oxidizing bacteria (AOB) until ammonia-oxidizing archaea (AOA) were discovered in 2005 (Könneke et al. 2005). Although initially characterized from marine environments, AOA are also present in terrestrial soils and are more abundant than AOB across a range of soils (Leininger et al. 2006). While prior work focused on grasslands and agricultural soils, their results nonetheless suggest a strong potential for archaea to be a major contributor to NH_4^+ oxidation in forest ecosystems, along with their bacterial counterpart. This potentially has highly influential implications for the current understanding of nitrification in terrestrial systems, which was previously focused on solely AOB. Nitrification has been studied for almost 150 years, yet AOA only recently been integrated into the literature (Sedlacek 2020). Consequently, we have a limited understanding of the environmental and ecological conditions in which AOA dominate nitrification in forest soils.

NH_4^+ oxidation is the first and rate-limiting step of nitrification (Frijlink et al. 1992, Hatzenpichler 2012), which controls the amount of NO_3^- available for plant uptake, as well as amounts leached to ground or surface water (Barnes et al. 1998). As such, understanding how AOA diversity and abundance varies across a landscape is important for understanding nutrient cycling in forests. Studies have shown that the abundance of AOA are influenced by environmental factors, such as pH and substrate availability (*i.e.,* NH_4^+; Nicol et al. 2008, Norman & Barrett 2014, Stempfhuber et al. 2015).

Soil pH strongly determines microbial community composition and biochemical activities (Alves et al. 2018, Nicol et al. 2008, Stempfhuber et al. 2015). Generally, AOB have a greater abundance than AOA at neutral or higher pH conditions, in which they significantly contribute to nitrification (Nicol et al. 2008, Norman & Barrett 2014, Shen et al. 2012, Stempfhuber et al. 2015). By contrast, in acidic conditions AOB abundance and activity decrease – cultivated AOB are incapable of surviving at pH < 7 (Nicol et al. 2008). Meanwhile, AOA are found to perform and sustain NH_4^+ oxidation in acidic soils, suggesting niche differentiation between AOA and AOB is likely determined by pH (Nicol et al. 2008, Norman & Barrett 2014,

Shen et al. 2012, Stempfhuber et al. 2015). These observations further suggest that the abundance of AOA should shift across a gradient of soil pH.

In addition to pH, microbial mineralization of plant litter and soil organic matter directly controls the availability of NH_4^+ in soil solution (Barnes et al. 1988), which, in turn, influences the relative contributions of AOA and AOB to nitrification. For example, Norman & Barrett (2014) observed that AOA are not limited by NH_4^+ availability, whereas AOB are. Low NH_4^+ availability limits the growth and activity of AOB, whereas high NH_4^+ availability inhibits the growth of AOA (Norman & Barrett 2014, Norman & Barrett 2016, Ouyang et al. 2017). This has potential implications for competitive interactions between AOA and AOB in soil, influencing AOA abundance. However, variation in NH_4^+ availability is often either linked to pH or the application of fertilizers in experimental studies. These observations ignore the potential influence of the natural supply of NH_4^+ by mineralization, which is absent in scientific literature.

We investigated how net N mineralization rates and soil pH influence the abundance and of AOA in temperate forest soils. Given the currently available information, we hypothesize that AOA abundance increases in relatively acidic forest soils with low N mineralization rates. We tested this idea against a null hypothesis, that the abundance and diversity of AOA do not change across a range of soil conditions. We addressed our hypotheses using a series of northern hardwood forest stands that span a natural gradient of net N mineralization.

2. Methods

2.1 Site Description and Sample Collection

Soil samples were collected in upland forests of northwestern Lower Michigan, in the Manistee National Forest. This research area and its N dynamics were initially described by Zak et al. (1986) and Zak et al. (1989), which demonstrated a natural gradient of net N mineralization and nitrification, across and within multiple ecosystem types.

In May 2019, 72 circular plots with 1-m radii were established in 12 forest stands, with 6 plots per site. These stands are in close proximity to each other – no more than 50 km apart – and are similar in climate, age (*ca.*100 years), and soil texture (~85% sand). We also selected plots near *Quercus rubra* (red oak) to minimize differences in litter biochemistry, which create variations in inorganic N availability. Six soil cores 2.5 cm in diameter were collected within each plot to a depth of 10 cm, which encompassed the Oe and A horizons. Interestingly, Leininger et al. (2006) found that relative abundance of AOA to AOB increases with increasing soil depth, especially past 40 cm. However, most roots take up nutrients within the first 10 cm from the soil surface. Thus, we chose to describe and quantify AOA populations within this depth, in which the products of NH_4^+ oxidation and nitrification would contribute the most to the available nutrient pool for plant uptake. The samples were then brought to the University of Michigan, where they were sieved and homogenized by hand. We determined current rates of net N mineralization and soil pH, while a subsample for each plot was stored at -80°C for DNA extraction.

2.2 Soil Properties and Nitrogen

The gradient of net N mineralization and soil pH was previously documented by Zak et al. (1989). We measured these soil properties to reconfirm patterned variation in NH_4^+ availability and pH for the present study. To determine net N mineralization, soil samples underwent a 28-day aerobic incubation period in the laboratory (Vitousek et al. 1982, Zak et al. 1989). Inorganic N (NO_3^- and NH_4^+) was measured before and after the incubation period using an AQ2 Discrete Analyzer (SEAL Analytical). Net N mineralization was calculated as the difference between final and initial concentrations of NO_3^- and NH_4^+. Although these determinations are potential rates for each site, Zak et al. (1989) demonstrated that laboratory mineralization potentials are highly correlated with *in situ* mineralization rates. Given this, we proceeded with these potentials as robust representations of mineralization rates in the field. Finally, soil pH was measured in the laboratory using a 1:1 slurry of 30 g of air-dried soil and deionized water.

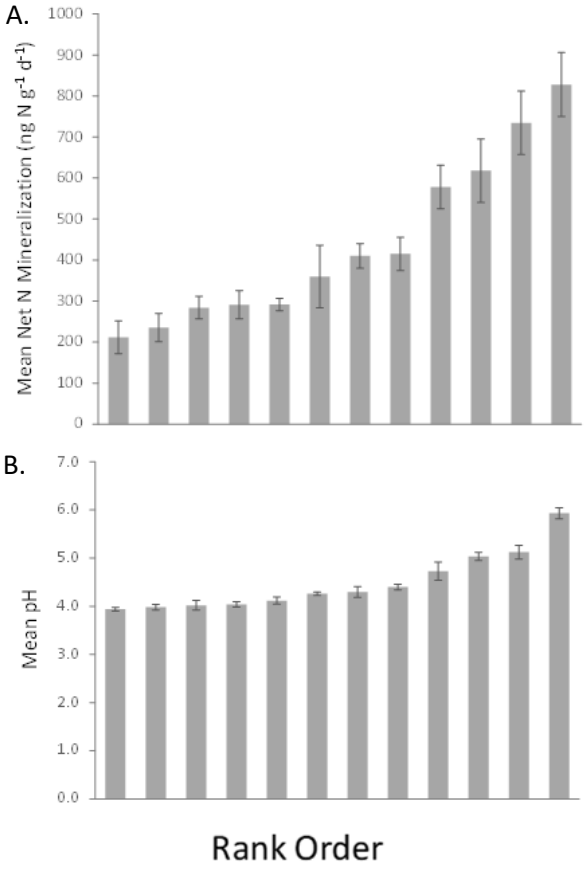

Figure 1. Rank order bar plots for mean net N mineralization (A) and pH (B) of the 12 northern hardwood forest study sites.

Results for net N mineralization rates show that these 12 sites span a gradient of inorganic N availability (Figure 1A), which is consistent with the findings of Zak et al. (1989). Across sites, mean net N mineralization range from 211 to 827 ng N g-1 d-1 (Table 1). By contrast, soil pH does not vary as strongly across the sites (Figure 1B). Soils are moderately acidic, mostly between 3.94 and 5.93 (Table 1).

Table 1. Summary of the stands based on Zak & Pregitzer (1990) and edaphic characteristics measured from the collected soil samples.
* indicates stands that had to be excluded from this study due to low PCR amplification.

Stand	Ecosystem Type	Mean Net N Mineralization (ng N g^{-1} d^{-1})	Mean pH
3*	Black oak-white oak/*Vaccinium*	291.16 ± 34.34	3.94 ± 0.04
9*	Black oak-white oak/*Vaccinium*	360.07 ± 75.90	4.30 ± 0.11
50*	Black oak-white oak/*Vaccinium*	235.16 ± 34.56	4.02 ± 0.10
58	Black oak-white oak/*Vaccinium*	291.59 ± 15.04	4.40 ± 0.06
7	Sugar maple-red oak/*Maianthemum*	410.16 ± 30.17	4.26 ± 0.04
20*	Sugar maple-red oak/*Maianthemum*	211.65 ± 40.04	4.04 ± 0.06
31*	Sugar maple-red oak/*Maianthemum*	283.8 ± 27.50	3.98 ± 0.06
41	Sugar maple-red oak/*Maianthemum*	578.02 ± 52.93	4.12 ± 0.08
6	Sugar maple-basswood/*Osmorhiza*	414.79 ± 40.65	5.03 ± 0.08
22	Sugar maple-basswood/*Osmorhiza*	827.97 ± 77.70	5.93 ± 0.12
24	Sugar maple-basswood/*Osmorhiza*	617.62 ± 77.24	5.12 ± 0.14
100	Sugar maple-basswood/*Osmorhiza*	734.57 ± 77.41	4.73 ± 0.19

2.3 Microbial Amplification and Sequencing

To detect AOA from the collected soil samples, we targeted the functional gene *amoA*, which encodes one of the subunits of NH_4^+ monooxygenase, a key enzyme in NH_4^+ oxidation (Leininger et al. 2006). Total genomic material was extracted from the soil using the DNeasy PowerLyzeer PowerSoil Kit (Qiagen, Germantown, MD, USA). The genomic DNA was subsequently purified using the DNeasy PowerClean CleanUp Kit (Qiagen). We verified its quality using a NanoDrop 8000 Spectrophotometer (Thermo Scientific) and gel electrophoresis (Argiroff et al. 2021).

To amplify the *amoA* region for AOA, we followed the PCR protocol by Aigle et al. (2019), with optimizations to the length and temperature of each step, amount of template, and primer concentration (Appendix D). We amplified the archaeal *amoA* sequence with sets of CrenamoA23f / CrenamoA616r primers for AOA (Table C1). We used unique primer combinations for each plot to avoid biases in amplification caused by primer-specific behaviors (Table C2). Additionally, we used Phusion High Fidelity DNA polymerase (New England Biolabs,

Ipswich, MA, USA) and modified the primers to include Illumina adaptors and barcodes for sequencing (Taylor et al. 2016).

The Illumina sequencing platform produces a relatively large number of short reads (Aigle et al. 2019) – this is advantageous to my study, which needed to maximize the number of reads of a highly specific functional gene from a comprehensive collection of environmental DNA. Because AOA primers produced 629 bp amplicons (Rotthauwe et al., 1997; Tourna et al., 2008) and the reads would be relatively short, an Illumina MiSeq 2 x 250 bp platform with Nano V2 chemistry was used for sequencing the archaeal *amoA* to generate paired end reads. This also offered greater flexibility in determining which of the paired reads – forward, reverse, or merged – to base subsequent analyses on, depending on the outcomes of sequence quality control checks. Additionally, sequencing primers with LNA (locked nucleic acids) oligonucleotides were utilized to increase the melting temperature (Qiagen). PCR libraries were normalized and purified with SequalPrep Normalization Plates.

Lastly, we excluded five stands from our amplicon analyses (3, 20, 31, 50, 9) because we did not observe amplification in the gel electrophoresis results for all, or all but one, of the plots within those stands. Such low amplification would result in insufficient sequence data. The 7 remaining stands (6, 7, 22, 24, 41, 58, 100) span a wide gradient of pH and net N mineralization and had a sufficient number of plots and sequence data following quality filtering, so subsequent analyses were based on these seven stands.

2.4 Bioinformatic Analysis

After obtaining the amplicon reads form the seven stands, we confirmed that the reads were *amoA* by conducting blastn, blastx and Fungene analyses. Additionally, the preliminary quality check of raw sequences using FastQC found that majority of forward and reverse reads were mostly of high quality (Q30 or greater). The reads were then quality-filtered and trimmed to remove primers, adaptors, and barcode sections with ‘cutadapt’ and the ‘DADA2’ package in R (Rosen et al. 2012; Callahan et al. 2016) to create amplicon sequence variants (ASVs). For the DADA2 pipeline, we used standard filtering parameters (maxN = 0, maxEE = c(2,2), truncQ = 2, minLen = 100, rm.phix = TRUE, compress = TRUE, multithread = FALSE) and dereplicated reads.

After these steps, one plot from stands 41, 58, and 100 each was removed due to low number of reads (< 15). This left 5 plots per stand for 41, 58, and 100, which was still sufficient for robust statistical analyses.

Following the DADA2 pipeline, USEARCH was used to remove non-*amoA* sequences and further check for chimeras with the UCHIME algorithm by comparing sequences against an archaeal *amoA* database provided by Alves et al. (2018) – only matched sequences were retained. While the same quality filtering procedure was performed on both forward and reverse reads up to this point, the reverse reads resulted in more unique reads than forward reads following this chimera removal process. As such, given that the reverse reads may provide more and higher quality data, subsequent analyses were only performed on the reverse reads. Finally, after extracting taxonomy information from the same database, taxonomy was assigned to the reverse reads in QIIME.

2.5 Phylogenetic Tree Construction

Phylogenetic placement of unique *amoA* ASVs was done by constructing maximum likelihood trees. A curated group of *amoA* reference sequences (Alves et al 2018) were aligned with our ASV reads using MAFFT (Katoh et al 2013) with the FFT-NS-2 method. Multiple sequence alignments were visually inspected for alignment to remove non-overlapping regions via msaTrim in R and re-aligned as before. Maximum likelihood trees were inferred using IQ-TREE (Nguyen et al 2015) with the GTR+F+I+Gamma4 model with Ultrafast bootstrap and SH-aLRT values calculated from 1000 replicates and perturbation at 0.1. Tree visualizations and annotations were created using the iTOL (https://itol.embl.de/ Letunic et al 2021).

2.6 Statistical Analysis

To explore how AOA communities are distributed relative to our gradients for pH and net N mineralization, AOA composition was evaluated across stands using nonmetric multidimensional scaling (NMDS) with Hellinger distances. Then, we performed a PERMANOVA using adonis2, Mantel tests, and TITAN analyses for both the pH and net N mineralization gradients. All tests were conducted in R with the phyloseq and vegan packages.

3. Results and Discussion

3.1 AOA abundance and diversity

Following Illumina MiSeq sequencing of the 7 remaining stands, a total of 652,331 reverse reads were obtained for AOA *amoA*. After quality filtering through the DADA2 pipeline and UCHIME, 591,226 of those reads remained (90% of the initial reads). At this point, 304 ASVs were identified. Alves et al. (2018) described 5 major lineages for AOA based on OTUs generated from *amoA*: *Ca.* Nitrosocaldales (NC), *Nitrososphaeales* (NS), *Ca.* Nitrosotaleales (NT), *Nitrosopumilales* (NP), and a small unassigned clade designated as *Incertae sedis* (NT/NP). Each lineage was further divided into broad subclades, designated by Greek letters. After assigning taxonomy to our ASVs, we found that the sequences in total represent 23 unique taxonomic groups, which are from clades belonging to two of the major lineages – NS and NT (Figure 2) – specifically the subclades NT-Alpha, NS-Beta, NS-Delta, NS-Gamma, and NS-Alpha (Figure 3). These results are consistent with the lineage characterizations by Alves et al. (2018), especially of each lineages' habitat specificity. The NS lineage is mostly specific to soils and sediment environments. Meanwhile, NT is evenly associated evenly with both soils and freshwater ecosystems – interestingly, the soil AOA from this lineage are associated with acidic conditions (generally soil pH <7.5 with more specific subclades detected in soil pH <6.5).

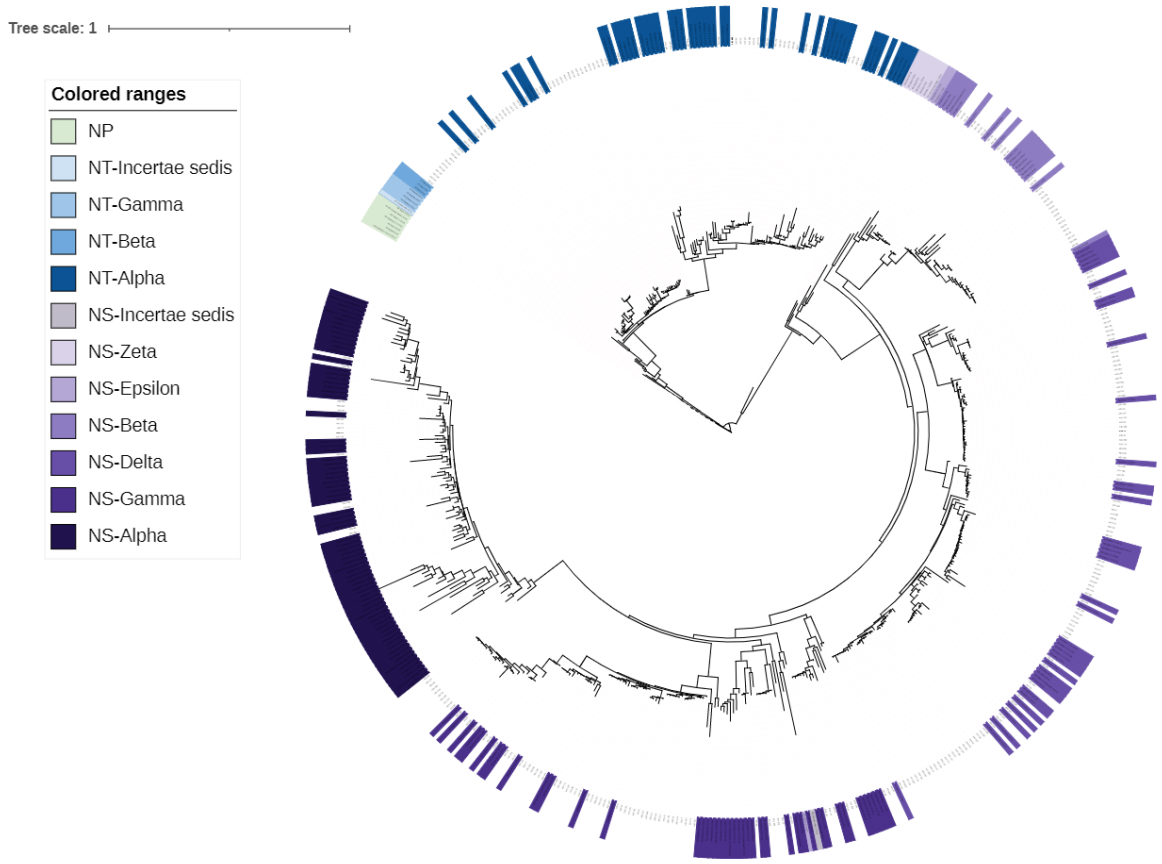

Figure 2. Circular maximum likelihood trees showing where the *amoA* AVS from stands 6, 7, 22, 24, 41, 58, 100 are placed relative to the known subclades described by Alves et al. (2018). The subclades, designated by a Greek letter and abbreviation of their order-level lineage, can be identified on the tree based on purple or blue labels. The white or empty spaces between them show where an ASV is placed on the tree.

Looking more closely at the stand level, the relative abundances of the lineages and subclades present in the samples were distinct across the landscape (Figure 3). The only stand of the Black oak-white oak/*Vaccinium* ecosystem type, stand 58 (Table 1), is primarily composed of AOA from the NT-Alpha subclade and minimally from the NS lineage. However, without AOA compositions for the remaining stands in that ecosystem type, we were unable to determine if the high relative abundance of NT-Alpha is unique for that stand or for the Black oak-white oak/*Vaccinium* ecosystem. For the other ecosystem types – Sugar maple-red oak/*Maianthemum* and Sugar maple-basswood/*Osmorhiza* – the NT lineage comprises no more than 50% of the AOA communities. Within the relatively acidic stands of the gradient, 7, 41, 58,

and 100 (Table 1), subclades NS-Gamma and NT-Alpha have the highest relative abundance (Figure 3). These patterns are supported by Titan analyses (Figure 5), which show that taxa within NS-Gamma and NT-Alpha are associated with low pH. The relative abundances of subclade within NS lineage also vary across stands, although NS-Gamma and NS-Delta are generally the most abundant of the NS groups present, followed by NS-Beta. To summarize, despite originating from upland forest sites in close proximity to each other, the AOA communities are highly distinct across stands.

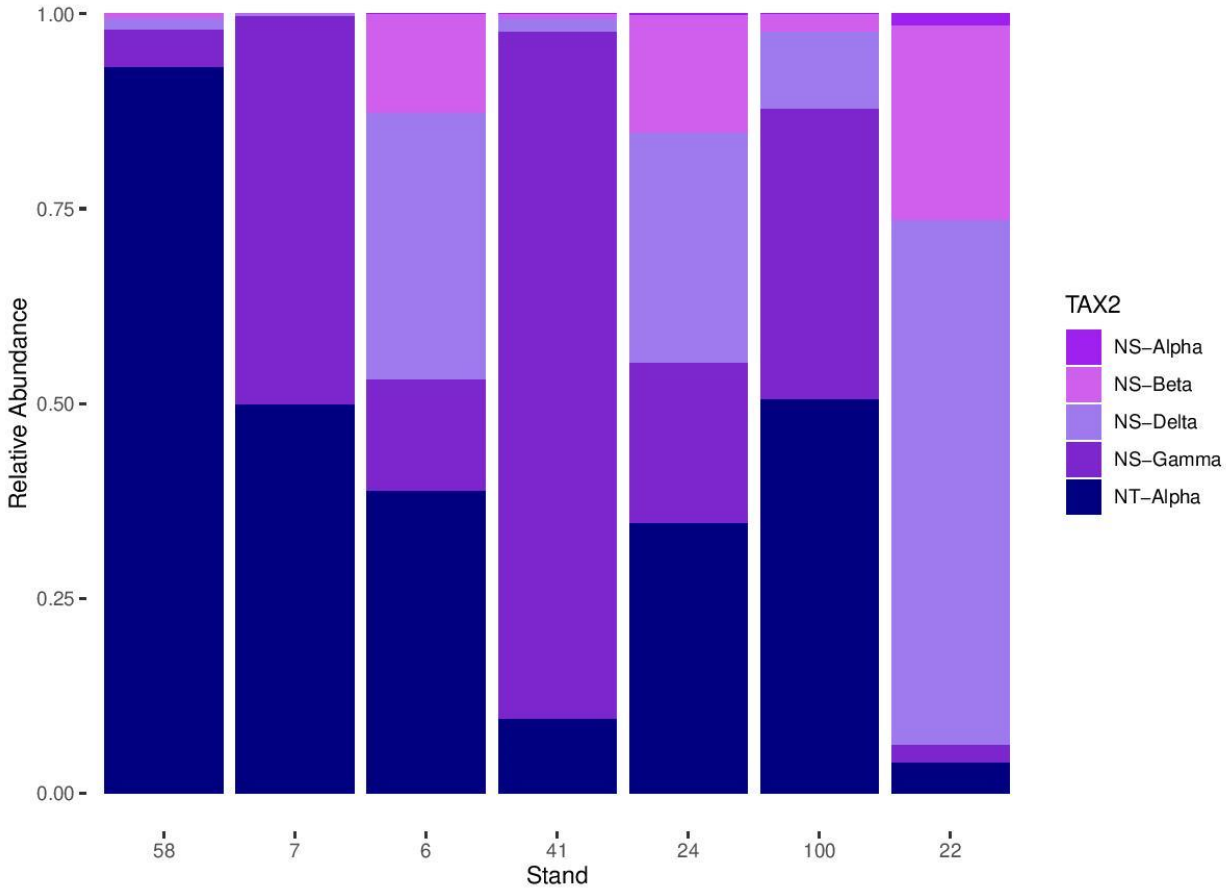

Figure 3. Stacked bar plot illustrating the relative abundance of AOA subclades present in each stand. Clades with relative abundances > 0.05% were removed from the figure.

3.2 Relative contributions of pH and mineralization

We conducted an NMDS as a preliminary analysis of beta diversity between stands and how AOA communities are distributed based on compositional dissimilarity (Figure 4). Then,

the NMDS biplot was supplemented with a PERMANOVA using the adonis2 function to determine whether AOA abundances and community composition between stands are significantly different based on groupings by pH or net N mineralization. We estimated a potential number of dimensions to include in the NMDS using a scree plot (Appendix F), which suggested 3 dimensions. This was supported by the stress values obtained for k=3 (~0.08) against k=2 (~0.15).

The results of the NMDS in Figure 4a show that AOA communities of the same stand are closely grouped together on similar sides of both axes. For instance, all 5 plots in stand 58 are clustered close to the center of axis 2 and near the bottom of axis 3. All 6 plots of stand 22 are clustered near the center of axis 3 and the right side of axis 2, and so on with other plots. This suggests that not only are plots of each stand potentially similar in AOA abundance and composition, but also that each stand may be distinguishable from each other based on their AOA composition – this would allow for the characterization sites based on their unique microbial composition.

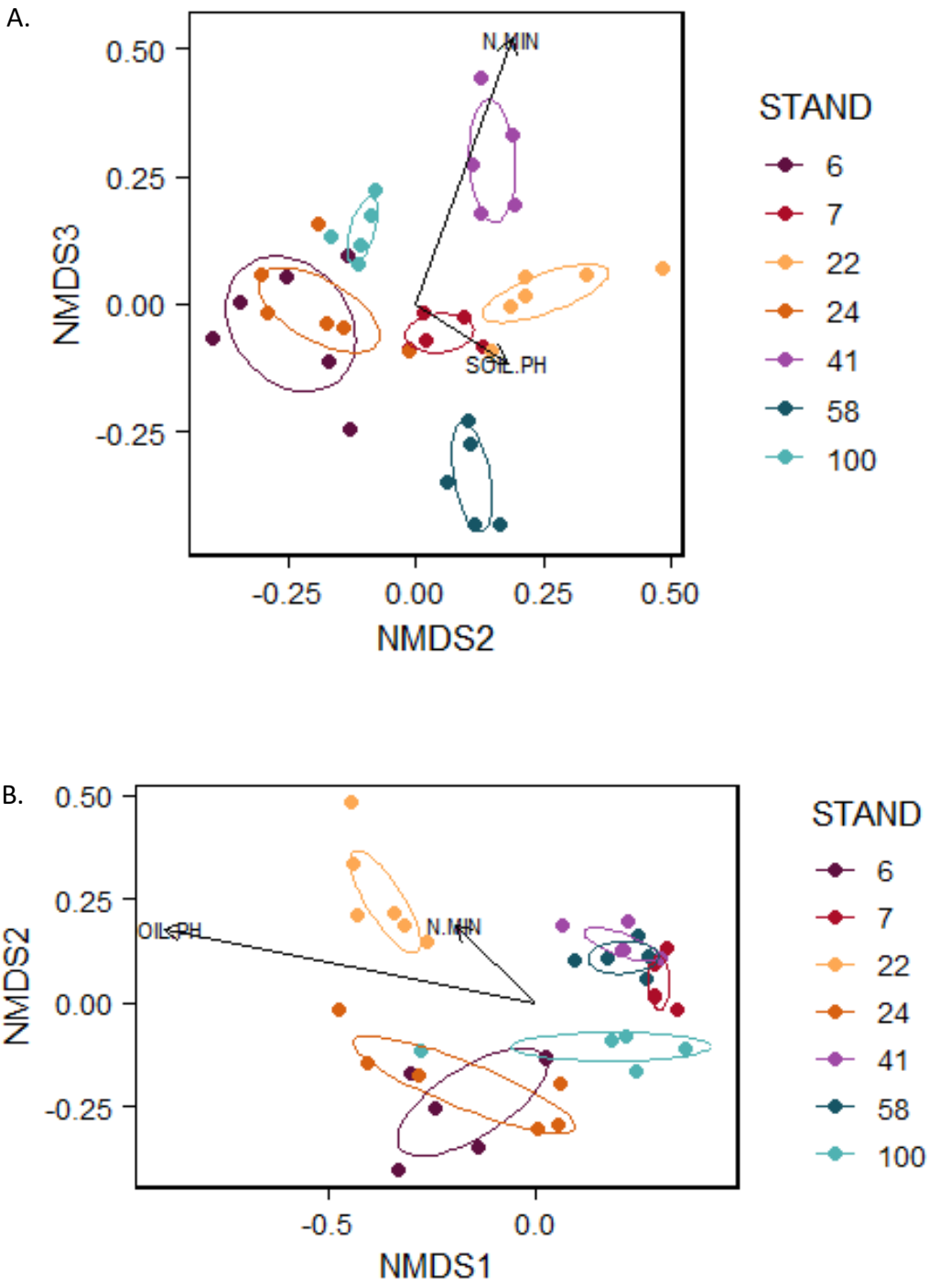

Figure 4. NMDS biplots of AOA communities by sample, grouped by stand. 2 out of 3 axes are displayed at a time. (A) shows dimensions 2 and 3, while (B) shows dimensions 1 and 2. Environmental vectors for pH and net N mineralization were made using envfit() and overlaid on the plot.

We tested several PERMANOVA models with a combination of potential contributing factors in addition to pH and net N mineralization, including total soil N and inorganic N (obtained from Argiroff et al. 2021). Additional predictors were included because of the potential influence of covariation between those variables, described by Argiroff et al. (2021). All of the tests demonstrate that pH and net N mineralization are significantly associated with differences in AOA diversity and community composition across sites ($p = 0.001$ and $p = 0.002$, respectively). The results were consistent, even after accounting for covariation between pH and mineralization rates (Appendix G). Additionally, while the R^2 values for each predictor varied across models, they commonly showed that pH contributes up to 23 % of the observed variation in community composition across the 7 stands, whereas net N mineralization contributes approximately only 8%. This provides evidence that pH is a more important predictive factor of AOA distribution than mineralization.

For the Mantel tests, the Spearman method was used, and Euclidean distances were calculated for pH and mineralization. The test for pH returned a significant association ($p < 0.001$), with an r statistic of 0.73. This indicates a significant strong positive correlation, showing that AOA communities that exist at close pH levels are more similar than AOA communities that are at different pH levels. This further supports that pH is an important factor associated with how AOA communities are distributed in the environment. For net N mineralization, the Mantel test also returned a low p value ($p = 0.003$), albeit with an r statistic of 0.17. This indicates a significant yet weak positive correlation – a conclusion that is consistent with the relative contributions of pH and mineralization revealed in the PERMANOVA results.

Overall, even though the range of mean pH across the Manistee stands was more constrained compared to pH ranges explored in previous studies (Nicol et al. 2008, Stempfhuber et al. 2015), these results continue to support pH as a strong determining factor of AOA abundance and composition, more so than mineralization. Tangentially, while not statistically tested, it is also notable that four of stands – 3, 20, 31, and 50 – which were excluded from analyses due to lack of amplification, had the lowest mean pH out of all other stands within the gradient (3.94, 4.04, 3.98, and 4.02, respectively). In follow-up analyses, it

would be worthwhile to investigate the potential influence of pH on the low AOA abundance (or lack of AOA) in these stands.

Finally, Titan analyses were conducted to show how the distribution of specific taxa assigned to our samples significantly changed across the spatial gradient of pH and net N mineralization. The analysis was conducted separately for pH and net N mineralization. While the PERMANOVA and Mantel tests established whether a significant association exists between these two predictors and our AOA community distribution as a whole, the Titan analyses helped to reveal the direction of those significant correlations (positive or negative) with AOA taxa within those communities.

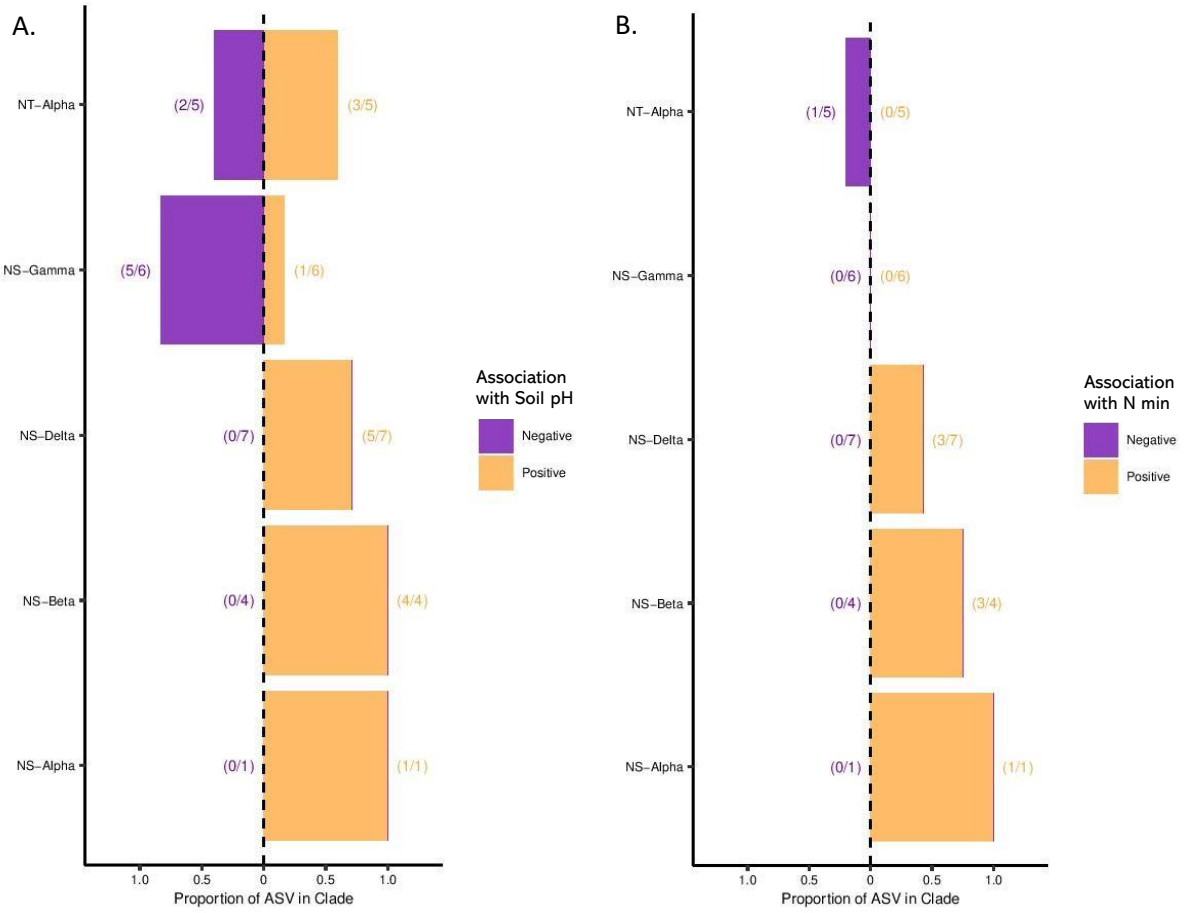

Figure 5. Results of Titan analyses on AOA clades for soil pH (A) and net N mineralization (B). Bars enumerate the clades for each lineage on the vertical axis that show a significant association to the tested environmental factor. A significant positive correlation is displayed in orange, extending to the right side of the plot. A significant negative correlation is displayed in

purple, extending to the left side of the plot. The number of significant clades out of total clades per lineage is adjacent to each bar.

The majority of unique taxa, 21 out of 23 taxa included in the analysis, across the 5 AOA subclades were significantly associated with changes in pH (Figure 5a). Of the subclades represented, NS-Delta, NS-Beta, and NS-Alpha have a positive correlation with pH, in which their abundances increase with increasing pH. This contradicts the hypothesis of this research, which states that AOA abundance increases at lower pH. However, 5 out of 6 taxa in NS-Gamma exhibit the opposite relationship as their abundances decrease as pH increases. This is supported by existing literature, as NS-Gamma in particular is known to be associated with acidic soil (Alves et al. 2018). The last subclade, NT-Alpha, which is the only subclade of the NT lineage represented here, shows taxa significantly associated with pH in both directions.

The TITAN results for net N mineralization mirror the results of the PERMANOVA and Mantel tests, in that mineralization does not appear to be strongly associated with differences in AOA community composition across stands. Compared to pH, only 8 out of the total 23 taxa are significantly associated with changes in net N mineralization (Figure 5b). Of the taxa that are significant, 7 clades (in the NS-Delta, NS-Beta, and NS-Alpha lineages) show a positive association: as net N mineralization increases, the abundances of these clades increase. Only one taxon in NT-Alpha shows a negative correlation. Again, this contradicts the original hypothesis, that AOA would be more abundant in forest soils with low mineralization rates.

Comparing these taxon-level associations with their relative abundances within stands, a number of stands (7, 41, 58, and 100) are primarily composed of NT-Alpha and NS-Gamma (Figure 3). These are the only two clades from the Titan analysis shown to have taxa with abundances that are negatively correlated with pH. Therefore, the communities for these stands, as a whole, may be more likely to have a negative response to increasing pH. By contrast, for stands 2, 22, and 24, taxa with abundances positively correlated with pH and mineralization (NS-Delta and NS-Beta) comprise a large fraction of the relative abundance for those stands. These AOA communities, especially stand 22 with the lowest relative NT-Alpha and NS-Gamma abundances, are likely exhibiting more positive responses to increasing pH and mineralization.

To summarize, the relative abundances of AOA taxa differ greatly between stands, and the AOA taxa themselves have contrasting associations to environmental variables such as pH or mineralization. A high relative abundance of a clade such as NS-Gamma in stand 41 provides support for our hypothesis. On the other hand, a high relative abundance of clades such as NS-Delta and NS-Beta in stand 22 provides evidence against our hypothesis. This demonstrates a large diversity of AOA responses to environmental variables that was not considered in the original hypothesis.

3.3 Enzyme kinetics of ammonia monooxygenase

While observed AOA communities in this study are diverse with unique compositions for each stand, it is unclear what is driving how these taxa are distributed across sites. A possible underlying mechanism may be the nitrifying enzyme kinetics that control the relative responses of NH_4^+ oxidizers to NH_4^+/NH_3 availability (Jung et al. 2022, Martens-Habbena et al. 2009). Enzyme kinetics can be described by Km – the half saturation constant which dictates substrate affinity of an enzyme – in which a low Km indicates high affinity for a substrate such as NH_4^+ (Auyeung et al. 2015).

Differences in Km between AOA and AOB could drive niche differentiation between the two organisms based on substrate availability, potentially influencing their relative abundance in the environment (Martens-Habbena et al. 2009). For instance, a strain of marine AOA, *Nitrosopumilus maritimus* SCM1, was the first described to have a Km of 133 nM NH_4^+, which is magnitudes lower than the Km of several marine AOB (Martens-Habbena et al. 2009). In this case, NH_4^+ monooxygenase for AOA requires lower concentrations of substrate to reach saturation compared to AOB, making this strain of AOA better adapted to substrate-limited environments. However, Jung et al. (2022) found that AOA exhibit a wide range of both NH_4^+ and NH_3 affinities across different environments and lineages, including affinities comparable to that of AOB. The NS lineage has the widest ranges of NH_3 affinities, whereas the NT lineage has a high affinity for NH_3, but a relatively low affinity for NH_4^+.

While the differences between NH_4^+ and NH_3 affinities may contribute to interesting interactions between AOA and substrate availability in more basic soils, in which NH_3 would be

more abundant, the pH range of soils in the Manistee stands precludes high concentrations of NH_3. As such, NH_4^+ is the dominant form in soil solution, and NH_4^+ affinities would drive niche differentiations between AOA and AOB as well as between taxa within AOA more so than NH_3 affinities. This would in turn influence their abundance and distributions. Therefore, there is a need to understand substrate affinities and distribution of AOB to fully capture the interactions between all NH_4^+ oxidizers that depend on NH_4^+ and/or NH_3 availability in the environment.

3.4 Incorporation into nutrient cycling

Because NH_4^+ oxidation is the rate-limiting step of nitrification, the distribution and activity of NH_4^+ oxidizers – such as AOA – across a landscape such as Manistee National Forest have a large influence on NO_3^- availability in the environment. Because AOA community composition varied highly across stands, they could potentially be contributing to varying nitrification rates, which also exists as a gradient across our study sites (Appendix B). However, only AOA communities were quantified in this study, excluding AOB. As such, we were incapable of determining associations between AOA communities and nitrification rates between stands without data on the abundance and distribution of AOB.

Therefore, to further understand how NH_4^+ oxidizers contribute to nutrient cycling, an important follow-up to this study is the incorporation of AOB abundance, which can be determined using the same procedures outlined for AOA. Studying AOB would also build on our understanding of AOA abundance, allowing for the determination of relative changes in diversity and composition between AOA and AOB across the same environmental gradients. With this additional information, it would be possible to investigate the relative contributions of AOA and AOB to nitrification. This would then connect the patterns observed between environmental variables and communities of NH_4^+ oxidizers to the broader context of nutrient cycling.

4. Conclusion

The relationship between AOA abundance, pH, and mineralization is nuanced and becomes more complex at lower taxonomic levels. Our hypothesis stated that AOA are more abundant in relatively acidic forest soils with low N mineralization rates. While the changes in AOA community composition were significantly correlated with changes in pH and net N mineralization, several AOA clades such as NS-Alpha, NS-Beta, and NS-Delta exhibited the opposite relationship stated in the hypothesis. These clades were determined to be significantly more abundant as pH and net N mineralization increased. On the other hand, NS-Gamma and two taxa from NT-Alpha displayed significant negative associations with pH that was consistent with our hypothesis. Meanwhile, net N mineralization in general is determined to be a relatively weak predictor of AOA distribution. This speaks to the diversity of environmental responses and taxa within AOA. Thus, based on these results, we recommend against generalizing the responses of AOA to environmental conditions, as they can be clade specific.

With a greater understanding of how AOA communities are assembled in the natural landscape, future research should focus on the distribution of AOB – another key organism responsible for NH_4^+ oxidation – across environmental gradients. Studying AOB alongside AOA will help uncover the contributions of pH and net N mineralization to interactions between the two types of NH_4^+ oxidizers, as well as their relative contributions to nitrification.

It is worth mentioning, though, that the analyses and descriptions of these AOA communities may be incomplete, because stands 3, 9, 20, 31, and 50 had to be cut from this study due to unobservable amplification from PCR. However, these stands notably have low or 0 mean nitrification rates (Appendix B) and the lowest mean pH (Table 1). This suggests that the lack of visual amplification may be associated with an absence or low presence of AOA in those stands in the first place. Therefore, it will be important to explore this pattern by supplementing the observations from PCR with quantitative evidence, such as from qPCR. Investigating why AOA communities are sparse in these sites may reveal more about how NH_4^+ oxidizers are distributed in the environment and why.

Through novel molecular techniques, this research successfully provided the first glimpse into AOA communities within natural environmental gradients. The study was able to

show that AOA communities of similar ecosystem types in close proximity to each other can be markedly distinct. These communities were also successfully categorized into known clades and lineages that are characteristic of acidic soil environments, and we were able to determine how the abundances of each taxon changed across environmental gradients. Building on this progress, future research based on the recommendations mentioned in this study will provide a more holistic view of nutrient cycling, revealing the enigmatic contributions of AOA to nitrification in natural ecosystems.

5. Appendices

Appendix A. Edaphic Characteristics of Manistee Plots (Argiroff et al. 2021)

PLOT	STAND	N.MIN ($\mu g\ N\ g^{-1}\ d^{-1}$)	NITRIFICATION ($\mu g\ NO_3^-\ g^{-1}\ d^{-1}$)	AMMONIUM ($\mu g\ NH_4^+\ g^{-1}\ d^{-1}$)	SOIL.PH
Plot_1	Stand_3	0.35290	0.00365	1.00660	4.03
Plot_2	Stand_3	0.32221	0.00000	0.11916	3.97
Plot_3	Stand_3	0.16809	0.00084	0.42135	3.87
Plot_4	Stand_3	0.22831	0.00000	0.00000	4.03
Plot_5	Stand_3	0.27782	-0.00268	0.21649	3.94
Plot_6	Stand_3	0.39760	-0.00105	0.00000	3.79
Plot_7	Stand_6	0.30192	0.30897	0.75466	5.09
Plot_8	Stand_6	0.49349	0.53602	1.42856	4.63
Plot_9	Stand_6	0.56952	0.61670	1.56039	5.13
Plot_10	Stand_6	0.35495	0.34664	0.00000	5.23
Plot_11	Stand_6	0.35908	0.32754	0.01198	5.07
Plot_12	Stand_6	0.40978	0.40421	0.17108	5.05
Plot_13	Stand_7	0.37972	0.01480	1.98267	4.11
Plot_14	Stand_7	0.51495	0.19668	1.98047	4.22
Plot_15	Stand_7	0.30211	0.06752	2.02178	4.26
Plot_16	Stand_7	0.43494	0.29217	2.45611	4.31
Plot_17	Stand_7	0.37541	0.18263	1.69257	4.31
Plot_18	Stand_7	0.45383	0.14037	2.46622	4.35
Plot_19	Stand_9	0.05007	-0.00091	1.57786	3.98
Plot_20	Stand_9	0.60685	0.69879	3.62396	4.72
Plot_21	Stand_9	0.42088	0.09921	9.51162	4.15
Plot_22	Stand_9	0.27160	0.00036	1.60547	4.11
Plot_23	Stand_9	0.39655	0.02059	3.60563	4.35
Plot_24	Stand_9	0.41447	0.02150	3.72722	4.48
Plot_25	Stand_20	0.31305	-0.00590	1.36998	3.78
Plot_26	Stand_20	0.19662	0.00104	0.00000	4
Plot_27	Stand_20	0.07871	0.00261	0.92679	4.1
Plot_28	Stand_20	0.34026	0.00077	1.21037	4.17
Plot_29	Stand_20	0.16873	-0.00023	0.00000	4.12
Plot_30	Stand_20	0.17252	-0.00123	0.37547	4.05
Plot_31	Stand_22	1.19134	1.21755	2.34614	6.34
Plot_32	Stand_22	0.84287	0.91415	2.64180	5.9
Plot_33	Stand_22	0.69365	0.70374	0.85692	6.22
Plot_34	Stand_22	0.73415	0.76991	1.55812	5.8
Plot_35	Stand_22	0.82630	0.90193	2.90760	5.69
Plot_36	Stand_22	0.67953	0.72328	2.05017	5.63
Plot_37	Stand_24	0.73728	0.89667	5.94295	4.79
Plot_38	Stand_24	0.93438	1.04434	5.15666	4.75
Plot_39	Stand_24	0.46952	0.50037	1.60211	4.96
Plot_40	Stand_24	0.52674	0.54193	0.82556	5.29

Plot_41	Stand_24	0.43328	0.43404	0.20373	5.65
Plot_42	Stand_24	0.60450	0.64868	1.70704	5.28
Plot_43	Stand_31	0.26180	-0.00214	1.04498	3.88
Plot_44	Stand_31	0.29798	0.00000	0.93423	4.01
Plot_45	Stand_31	0.40544	0.00321	2.84143	3.93
Plot_46	Stand_31	0.27555	-0.00067	1.42946	3.9
Plot_47	Stand_31	0.20296	-0.00049	2.01591	3.9
Plot_48	Stand_31	0.25908	0.00187	0.70909	4.26
Plot_49	Stand_41	0.56756	0.51660	2.16691	3.94
Plot_50	Stand_41	0.47878	0.49186	0.78136	4.06
Plot_51	Stand_41	0.72361	0.71611	1.63042	4.3
Plot_52	Stand_41	0.63386	0.33406	2.08086	4.24
Plot_53	Stand_41	0.38120	0.19578	1.93072	3.87
Plot_54	Stand_41	0.68313	0.67633	2.69683	4.29
Plot_55	Stand_50	0.34398	0.00109	2.76928	4.4
Plot_56	Stand_50	0.18337	0.00000	0.87203	4.05
Plot_57	Stand_50	0.14624	0.00272	0.24498	3.67
Plot_58	Stand_50	0.24550	-0.00295	0.27957	3.94
Plot_59	Stand_50	0.32673	-0.00258	0.04738	3.93
Plot_60	Stand_50	0.16517	-0.00026	0.08623	4.13
Plot_61	Stand_58	0.22629	-0.00009	0.90112	4.2
Plot_62	Stand_58	0.28134	0.00724	0.90320	4.37
Plot_63	Stand_58	0.30334	0.00762	2.30426	4.46
Plot_64	Stand_58	0.33367	0.03944	2.51937	4.44
Plot_65	Stand_58	0.31421	0.04029	0.58252	4.61
Plot_66	Stand_58	0.29067	0.05097	2.56060	4.31
Plot_67	Stand_100	0.52663	0.56681	1.69407	4.4
Plot_68	Stand_100	0.76474	0.79214	1.19219	4.23
Plot_69	Stand_100	1.02725	1.05376	3.00922	4.44
Plot_70	Stand_100	0.86050	0.82781	4.16338	4.74
Plot_71	Stand_100	0.66473	0.75007	3.07810	5.18
Plot_72	Stand_100	0.56358	0.60387	1.48229	5.38

Appendix B. Mean Nitrification Rates

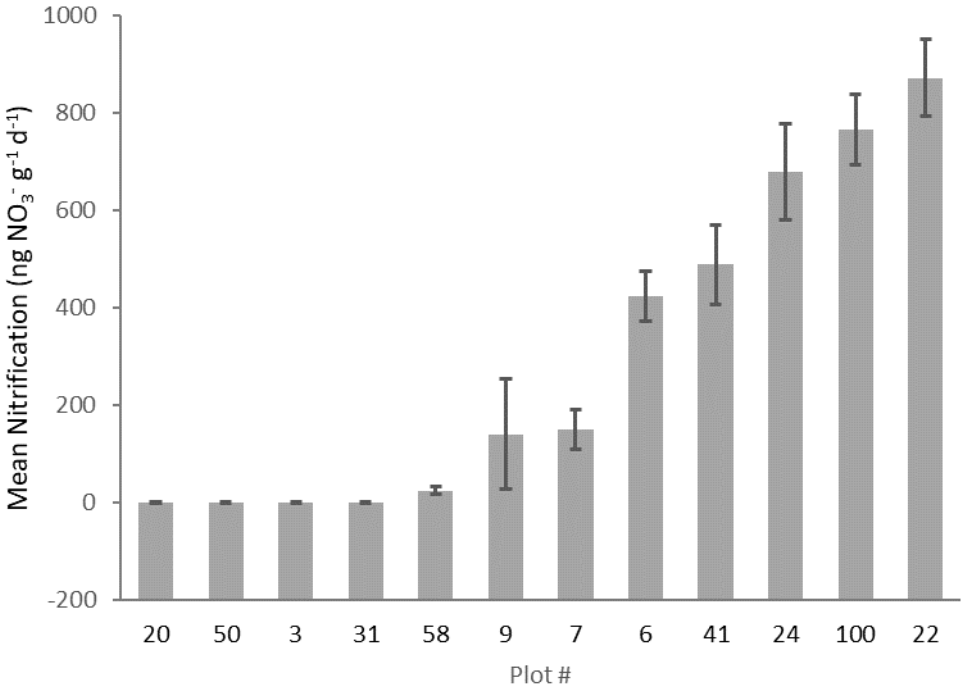

Figure B1. Mean nitrification rates per plot, ordered from lowest to highest rates. Nitrification was determined concurrently with net N mineralization, from the inorganic N measurements collected from the 28-day incubation period of the soil samples. Nitrification rates were calculated as the increase in extractable NO3- per day during the incubation period.

Appendix C. *amoA* Primers and Primer Combinations

Table C1. AOA *amoA* reverse primers

Forward Primer Name	Reverse Primer Name
SA502amoaA	SA701amoaA
SA503amoaA	SA702amoaA
SA504amoaA	SA703amoaA
SA505amoaA	SA704amoaA
SA508amoaA	SA705amoaA
SB501amoaA	SA706amoaA
SB503amoaA	SA709amoaA
SB502amoaA	SA712amoaA
SB504amoaA	SB702amoaA
	SB703amoaA

Table C2. Unique primer combinations used for each sample

Stand	Plot	Forward primer	Reverse primer
3	1	SA503	SA703
	2	SB503	SA701
	3	SA503	SA706
	4	SA504	SA705
	5	SB503	SA705
	6	SA503	SA701
6	7	SB501	SA706
	8	SB504	SA712
	9	SB503	SA704
	10	SB504	SA702
	11	SA505	SA703
	12	SB502	SA701
7	13	SB502	SA708
	14	SA508	SA708
	15	SB501	SA702
	16	SB501	SB703
	17	SB504	SB703
	18	SB504	SA703
24	37	SB501	SA703
	38	SA502	SA703
	39	SA505	SA706
	40	SB501	SA708
	41	SA502	SA701
	42	SA503	SB702
31	43	SA505	SA705
	44	SB504	SA705
	45	SA508	SA704
	46	SA503	SA712
	47	SA503	SA708
	48	SA503	SA704
41	49	SA504	SA701
	50	SA508	SB703
	51	SA505	SA712
	52	SB502	SA703
	53	SA504	SA702
	54	SA508	SA703

9	19	SA508	SB702
	20	SA502	SA708
	21	SA502	SB702
	22	SB503	SB702
	23	SA504	SB702
	24	SB504	SA706
20	25	SB503	SB703
	26	SA508	SA705
	27	SA505	SA701
	28	SA504	SA704
	29	SB503	SA708
	30	SA504	SA712
22	31	SA504	SB703
	32	SA502	SB703
	33	SB501	SA704
	34	SB503	SA702
	35	SB502	SA706
	36	SB504	SA706

50	55	SB502	SA704
	56	SB504	SB702
	57	SA502	SA702
	58	SA503	SA705
	59	SA504	SA706
	60	SA508	SA712
58	61	SB503	SA706
	62	SB502	SB702
	63	SA502	SA705
	64	SA505	SA708
	65	SA505	SB703
	66	SB503	SA703
100	67	SA502	SA706
	68	SB501	SA712
	69	SA505	SA702
	70	SA508	SA701
	71	SB503	SA712
	72	SB502	SA705

Appendix D. PCR Reagents and Thermocycler Settings

Table D1. AOA *amoA* reagents used in a PCR reaction (top), and the PCR thermoprofile (bottom) adapted for greatest amplification results.

Reagent	Volume (µL)
5X Phusion buffer	5
2mM dNTP	2.5
(5µM) forward primer	1
(5µM) reverse primer	1
(20mg/mL) BSA	0.5
Phusion Taq	0.5
Nuclease free H_2O	13.5
DNA template	1
Total	25

Step	Temp (C)	Time	Cycle
Initial denaturation	95	5 minutes	-
Denaturation	95	20 seconds	27 cycles
Annealing	64	45 seconds	
Extension	72	45 seconds	
Final extension	72	10 minutes	-

Appendix E. AOA Assigned Taxonomic Table

Total Sequences	Taxon
185	NS;NS_OTU1
87	NS;NS-Alpha;NS-Alpha-3;NS-Alpha-3.2;NS-Alpha-3.2.1;NS-Alpha-3.2.1.1;NS-Alpha-3.2.1.1.1;NS-Alpha-3.2.1.1.1.2;NS-Alpha-3.2.1.1.1.2_OTU2
3	NS;NS-Alpha;NS-Alpha-3;NS-Alpha-3.2;NS-Alpha-3.2.1;NS-Alpha-3.2.1.1;NS-Alpha-3.2.1.1.1;NS-Alpha-3.2.1.1.1.2;NS-Alpha-3.2.1.1.1.2_OTU3
89	NS;NS-Alpha;NS-Alpha-3;NS-Alpha-3.2;NS-Alpha-3.2.3;NS-Alpha-3.2.3.1;NS-Alpha-3.2.3.1.1;NS-Alpha-3.2.3.1.1_OTU9
97	NS;NS-Alpha;NS-Alpha-3;NS-Alpha-3.2;NS-Alpha-3.2.3;NS-Alpha-3.2.3.1;NS-Alpha-3.2.3.1.3;NS-Alpha-3.2.3.1.3_OTU1
3	NS;NS-Alpha;NS-Alpha-3;NS-Alpha-3.2;NS-Alpha-3.2.3;NS-Alpha-3.2.3.1;NS-Alpha-3.2.3.1.4;NS-Alpha-3.2.3.1.4.2;NS-Alpha-3.2.3.1.4.2_OTU3
544	NS;NS-Alpha;NS-Alpha-3;NS-Alpha-3.2;NS-Alpha-3.2.3;NS-Alpha-3.2.3.1;NS-Alpha-3.2.3.1.4;NS-Alpha-3.2.3.1.4_OTU3
911	NS;NS-Alpha;NS-Alpha-3;NS-Alpha-3.2;NS-Alpha-3.2.3;NS-Alpha-3.2.3.1;NS-Alpha-3.2.3.1.7;NS-Alpha-3.2.3.1.7_OTU5
16	NS;NS-Alpha;NS-Alpha-3;NS-Alpha-3.2;NS-Alpha-3.2.3;NS-Alpha-3.2.3.1;NS-Alpha-3.2.3.1.7;NS-Alpha-3.2.3.1.7_OTU6
38	NS;NS-Alpha;NS-Alpha-3;NS-Alpha-3.2;NS-Alpha-3.2.3;NS-Alpha-3.2.3.1;NS-Alpha-3.2.3.1_OTU2
14031	NS;NS-Beta;NS-Beta-1;NS-Beta-1_OTU10
41	NS;NS-Beta;NS-Beta-1;NS-Beta-1_OTU12
18038	NS;NS-Beta;NS-Beta-1;NS-Beta-1_OTU6
15300	NS;NS-Beta;NS-Beta-1;NS-Beta-1_OTU9
18777	NS;NS-Beta;NS-Beta-2;NS-Beta-2_OTU1
28519	NS;NS-Delta;NS-Delta-1;NS-Delta-1.1;NS-Delta-1.1.2;NS-Delta-1.1.2.1;NS-Delta-1.1.2.1_OTU13
2600	NS;NS-Delta;NS-Delta-1;NS-Delta-1.1;NS-Delta-1.1.3;NS-Delta-1.1.3_OTU2
1330	NS;NS-Delta;NS-Delta-1;NS-Delta-1.2;NS-Delta-1.2.1;NS-Delta-1.2.1_OTU3
156	NS;NS-Delta;NS-Delta-1;NS-Delta-1.2;NS-Delta-1.2.1;NS-Delta-1.2.1_OTU5
113	NS;NS-Delta;NS-Delta-1;NS-Delta-1.2;NS-Delta-1.2.2;NS-Delta-1.2.2_OTU2
51135	NS;NS-Delta;NS-Delta-1;NS-Delta-1.Incertae_sedis.3;NS-Delta-1.Incertae_sedis.3_OTU2
163	NS;NS-Delta;NS-Delta-1;NS-Delta-1_OTU4
10618	NS;NS-Delta;NS-Delta-1;NS-Delta-1_OTU7
43566	NS;NS-Delta;NS-Delta-2;NS-Delta-2.1;NS-Delta-2.1_OTU2
1243	NS;NS-Delta;NS-Delta-2;NS-Delta-2.2;NS-Delta-2.2.1;NS-Delta-2.2.1_OTU2
2551	NS;NS-Delta;NS-Delta-2;NS-Delta-2.2;NS-Delta-2.2.1;NS-Delta-2.2.1_OTU4
382	NS;NS-Delta;NS-Delta-2;NS-Delta-2.2;NS-Delta-2.2.1;NS-Delta-2.2.1_OTU5

214	NS;NS-Gamma;NS-Gamma-2;NS-Gamma-2.1;NS-Gamma-2.1.2;NS-Gamma-2.1.2.2;NS-Gamma-2.1.2.2_OTU3
147	NS;NS-Gamma;NS-Gamma-2;NS-Gamma-2.2;NS-Gamma-2.2.3;NS-Gamma-2.2.3_OTU3
435	NS;NS-Gamma;NS-Gamma-2;NS-Gamma-2.3;NS-Gamma-2.3.2;NS-Gamma-2.3.2.2;NS-Gamma-2.3.2.2_OTU1
6765	NS;NS-Gamma;NS-Gamma-2;NS-Gamma-2.3;NS-Gamma-2.3.2;NS-Gamma-2.3.2.2;NS-Gamma-2.3.2.2_OTU3
8088	NS;NS-Gamma;NS-Gamma-2;NS-Gamma-2.3;NS-Gamma-2.3.2;NS-Gamma-2.3.2.2;NS-Gamma-2.3.2.2_OTU6
5793	NS;NS-Gamma;NS-Gamma-2;NS-Gamma-2.3;NS-Gamma-2.3.2;NS-Gamma-2.3.2.2;NS-Gamma-2.3.2.2_OTU8
2628	NS;NS-Gamma;NS-Gamma-2;NS-Gamma-2.3;NS-Gamma-2.3.2;NS-Gamma-2.3.2.3;NS-Gamma-2.3.2.3_OTU3
6	NS;NS-Gamma;NS-Gamma-2;NS-Gamma-2.3;NS-Gamma-2.3.2;NS-Gamma-2.3.2_OTU1
114620	NS;NS-Gamma;NS-Gamma-2;NS-Gamma-2.3;NS-Gamma-2.3.2;NS-Gamma-2.3.2_OTU2
1288	NS;NS-Gamma;NS-Gamma-2;NS-Gamma-2.3;NS-Gamma-2.3_OTU2
1001	NT;NT-Alpha;NT-Alpha_OTU10
245	NT;NT-Alpha;NT-Alpha_OTU5
151	NT;NT-Alpha;NT-Alpha_OTU6
3201	NT;NT-Alpha;NT-Alpha_OTU7
132	NT;NT-Alpha;NT-Alpha_OTU8
7	NT;NT-Alpha;NT-Alpha-1;NT-Alpha-1.1;NT-Alpha-1.1.1;NT-Alpha-1.1.1.1;NT-Alpha-1.1.1.1.1;NT-Alpha-1.1.1.1.1_OTU3
9	NT;NT-Alpha;NT-Alpha-1;NT-Alpha-1.1;NT-Alpha-1.1.1;NT-Alpha-1.1.1.1;NT-Alpha-1.1.1.1.2;NT-Alpha-1.1.1.1.2_OTU4
161939	NT;NT-Alpha;NT-Alpha-1;NT-Alpha-1.1;NT-Alpha-1.1.1;NT-Alpha-1.1.1.1;NT-Alpha-1.1.1.1.3;NT-Alpha-1.1.1.1.3.2;NT-Alpha-1.1.1.1.3.2.Incertae_sedis;NT-Alpha-1.1.1.1.3.2.Incertae_sedis_OTU1
10	NT;NT-Alpha;NT-Alpha-1;NT-Alpha-1.1;NT-Alpha-1.1.1;NT-Alpha-1.1.1.1;NT-Alpha-1.1.1.1.3;NT-Alpha-1.1.1.1.3_OTU1
1205	NT;NT-Alpha;NT-Alpha-1;NT-Alpha-1.1;NT-Alpha-1.1.1;NT-Alpha-1.1.1.1;NT-Alpha-1.1.1.1.Incertae_sedis;NT-Alpha-1.1.1.1.Incertae_sedis_OTU1
93	NT;NT-Alpha;NT-Alpha-1;NT-Alpha-1.1;NT-Alpha-1.1.1;NT-Alpha-1.1.1.1;NT-Alpha-1.1.1.1_OTU4
4499	NT;NT-Alpha;NT-Alpha-1;NT-Alpha-1.1;NT-Alpha-1.1.1;NT-Alpha-1.1.1.2;NT-Alpha-1.1.1.2_OTU3
85	NT;NT-Alpha;NT-Alpha-1;NT-Alpha-1.1;NT-Alpha-1.1.2;NT-Alpha-1.1.2.2;NT-Alpha-1.1.2.2_OTU5
70	NT;NT-Alpha;NT-Alpha-1;NT-Alpha-1.2;NT-Alpha-1.2.1;NT-Alpha-1.2.1_OTU4
58879	NT;NT-Alpha;NT-Alpha-Incertae_sedis;NT-Alpha-Incertae_sedis_OTU2

Appendix F. NMDS Scree and Stress Plot

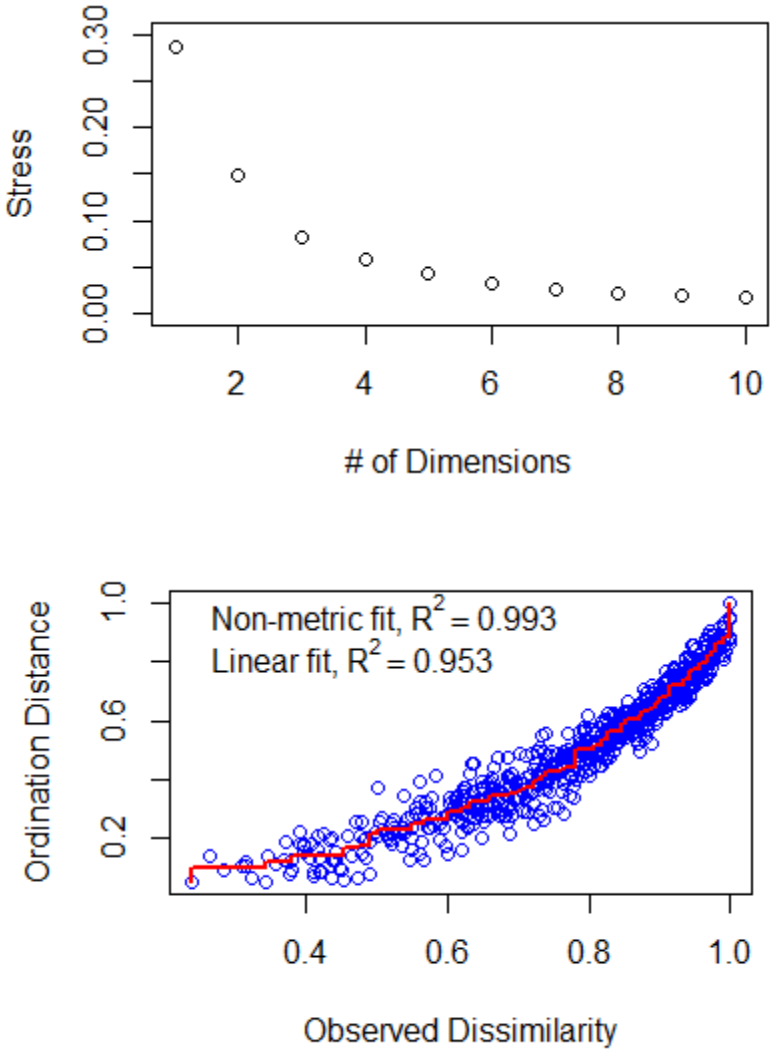

Figure F1. Scree plot (above) showing an elbow at 3 dimensions, below a stress value of 0.10. Stress plot (below) showing a strong correlation between the observed dissimilarity and ordination distance with 3 dimensions.

Appendix G. adonis PERMANOVA models

Figure G1. PERMANOVA model results with all environmental variables, including covariation between soil pH and N mineralization.

```
Permutation test for adonis under reduced model
Terms added sequentially (first to last)
Permutation: free
Number of permutations: 999

adonis2(formula = hellinger_dist_matrix ~ SOIL.PH + N.MIN + SPEC.TOTAL.N +
 N.INORG + SOIL.PH * N.MIN, data = site_factors)
              Df SumOfSqs      R2       F Pr(>F)
SOIL.PH        1   2.7354 0.23425 13.3266  0.001 ***
N.MIN          1   0.9570 0.08195  4.6623  0.001 ***
SPEC.TOTAL.N   1   0.7549 0.06465  3.6777  0.004 **
N.INORG        1   0.2772 0.02374  1.3504  0.203
SOIL.PH:N.MIN  1   0.3847 0.03294  1.8741  0.065 .
Residual      32   6.5683 0.56248
Total         37  11.6774 1.00000
---
Signif. codes:  0 ‘***’ 0.001 ‘**’ 0.01 ‘*’ 0.05 ‘.’ 0.1 ‘ ’ 1
```

Figure G1. PERMANOVA model results with all environmental variables, including covariation between soil pH and N mineralization.

```
Permutation test for adonis under reduced model
Terms added sequentially (first to last)
Permutation: free
Number of permutations: 999

adonis2(formula = hellinger_dist_matrix ~ SOIL.PH + N.MIN + SPEC.TOTAL.N +
 N.INORG, data = site_factors)
             Df SumOfSqs      R2       F Pr(>F)
SOIL.PH       1   2.7354 0.23425 12.9827  0.001 ***
N.MIN         1   0.9570 0.08195  4.5420  0.001 ***
SPEC.TOTAL.N  1   0.7549 0.06465  3.5828  0.002 **
N.INORG       1   0.2772 0.02374  1.3155  0.229
Residual     33   6.9530 0.59542
Total        37  11.6774 1.00000
---
Signif. codes:  0 ‘***’ 0.001 ‘**’ 0.01 ‘*’ 0.05 ‘.’ 0.1 ‘ ’ 1
```

Figure G2. PERMNAOVA model with all environmental variables, without accounting for covariation

```
Permutation test for adonis under reduced model
Terms added sequentially (first to last)
Permutation: free
Number of permutations: 999

adonis2(formula = hellinger_dist_matrix ~ N.MIN + SPEC.TOTAL.N + SOIL.PH +
 SOIL.PH * N.MIN, data = site_factors)
              Df SumOfSqs      R2      F Pr(>F)
N.MIN          1   0.9746 0.08346 4.7127  0.001 ***
SPEC.TOTAL.N   1   1.9426 0.16636 9.3937  0.001 ***
SOIL.PH        1   1.5301 0.13103 7.3989  0.001 ***
N.MIN:SOIL.PH  1   0.4058 0.03475 1.9622  0.034 *
Residual      33   6.8244 0.58441
Total         37  11.6774 1.00000
---
Signif. codes:  0 ‘***’ 0.001 ‘**’ 0.01 ‘*’ 0.05 ‘.’ 0.1 ‘ ’ 1
```

Figure G3. PERMNAOVA model with all environmental variables in a different order, which results in different R-squared and F statistics from those of Figure G1.

```
Permutation test for adonis under reduced model
Terms added sequentially (first to last)
Permutation: free
Number of permutations: 999

adonis2(formula = hellinger_dist_matrix ~ SOIL.PH + N.MIN + SOIL.PH * N.MIN,
 data = site_factors)
              Df SumOfSqs      R2       F Pr(>F)
SOIL.PH        1   2.7354 0.23425 13.0577  0.001 ***
N.MIN          1   0.9570 0.08195  4.5682  0.001 ***
SOIL.PH:N.MIN  1   0.8625 0.07386  4.1172  0.001 ***
Residual      34   7.1225 0.60994
Total         37  11.6774 1.00000
---
Signif. codes:  0 ‘***’ 0.001 ‘**’ 0.01 ‘*’ 0.05 ‘.’ 0.1 ‘ ’ 1
```

Figure G4. PERMNAOVA model with only soil pH and N mineralization, accounting for their covariance.

6. Literature Cited

1. **Aigle, A., Prosser, J. I., & Gubry-Rangin, C. (2019).** The application of high-throughput sequencing technology to analysis of amoA phylogeny and environmental niche specialisation of terrestrial bacterial ammonia-oxidisers. Environmental Microbiomes, 14(1), 1–10. https://doi.org/10.1186/s40793-019-0342-6
2. **Alves, R. J. E., Minh, B. Q., Urich, T., von Haeseler, A., & Schleper, C. (2018).** Unifying the global phylogeny and environmental distribution of ammonia-oxidising archaea based on amoA genes. Nature Communications 2018 9:1, 9(1), 1–17. https://doi.org/10.1038/s41467-018-03861-1
3. **Argiroff, W. A., Zak, D. R., Pellitier, P. T., Upchurch, R. A., Belke, J. P. (2021).** Decay by ectomycorrhizal fungi couples soil organic matter to nitrogen availability. Ecology Letters. 2021;00:1-14. DOI: 10.1111/ele.13923.
4. **Auyeung, D. S. N., Martiny, J. B. H., & Dukes, J. S. (2015).** Nitrification kinetics and ammonia-oxidizing community respond to warming and altered precipitation. Ecosphere, 6(5), art83.
5. **Barnes, B. V., Zak, D. R., Denton, S. R., Spurr, S. H. (1998).** Forest ecology. 4th ed. New York: Wiley.
6. **Callahan, B. J., McMurdie, P. J., Rosen, M. J., Han, A. W., Johnson, A. J. A., & Holmes, S. P. (2016).** DADA2: high-resolution sample inference from Illumina amplicon data. Nature methods, 13(7), 581-583.
7. **Fish, J. A., Chai, B., Wang, Q., Sun, Y., Brown, C. T., Tiedje, J. M., & Cole, J. R. (2013).** FunGene: the functional gene pipeline and repository. Frontiers in microbiology, 4, 291.
8. **Frijlink, M. J., Abee, T., Laanbroek, H. J., de Boer, W., & Konings, W. N. (1992).** The bioenergetics of ammonia and hydroxylamine oxidation in Nitrosomonas europaea at acid and alkaline pH. Archives of Microbiology, 157(2), 194-199.
9. **Hatzenpichler, R. (2012).** Diversity, physiology, and niche differentiation of ammonia-oxidizing archaea. Applied and environmental microbiology, 78(21), 7501-7510.
10. **Jung, M. Y., Sedlacek, C. J., Kits, K. D., Mueller, A. J., Rhee, S. K., Hink, L., Nicol, G. W., Bayer, B., Lehtovirta-Morley, L., Wright, C., de la Torre, J. R., Herbold, C. W., Pjevac, P.,**

Daims, H., & Wagner, M. (2022). Ammonia-oxidizing archaea possess a wide range of cellular ammonia affinities. ISME Journal, 16(1), 272–283. https://doi.org/10.1038/s41396-021-01064-z

11. **Kalyaanamoorthy, S., Minh, B., Wong, T. et al. (2017).** ModelFinder: fast model selection for accurate phylogenetic estimates. Nat Methods 14, 587–589.
12. **Katoh, K., Kuma, K. I., Toh, H., & Miyata, T. (2005).** MAFFT version 5: improvement in accuracy of multiple sequence alignment. Nucleic acids research, 33(2), 511-518.
13. **Könneke, M., Bernhard, A., de la Torre, J., Walker, C. B., Waterbury, J. B., Stahl, D. A. (2005).** Isolation of an autotrophic ammonia-oxidizing marine archaeon. Nature 437, 543–546. https://doi.org/10.1038/nature03911
14. **Leininger, S., Urich, T., Schloter, M., Schwark, L., Qi, J., Nicol, G. W., Prosser, J. I., Schuster, S. C., & Schleper, C. (2006).** Archaea predominate among ammonia-oxidizing prokaryotes in soils. Nature, 442(7104), 806–809. https://doi.org/10.1038/nature04983
15. **Letunic, I. & Bork, P. (2021).** Interactive Tree Of Life (iTOL) v5: an online tool for phylogenetic tree display and annotation. Nucleic acids research 49.W1: W293-W296.
16. **Martens-Habbena, W., Berube, P. M., Urakawa, H., De La Torre, J. R., & Stahl, D. A. (2009).** Ammonia oxidation kinetics determine niche separation of nitrifying Archaea and Bacteria. Nature, 461(7266), 976–979.
17. **Nicol, G. W., Leininger, S., Schleper, C., & Prosser, J. I. (2008).** The influence of soil pH on the diversity, abundance and transcriptional activity of ammonia oxidizing archaea and bacteria. Environmental Microbiology, 10(11), 2966–2978. https://doi.org/10.1111/j.1462-2920.2008.01701.x
18. **Norman, J. S., & Barrett, J. E. (2014).** Substrate and nutrient limitation of ammonia-oxidizing bacteria and archaea in temperate forest soil. Soil Biology and Biochemistry, 69, 141–146. https://doi.org/10.1016/j.soilbio.2013.11.003
19. **Norman, J. S., & Barrett, J. E. (2016).** Substrate availability drives spatial patterns in richness of ammonia-oxidizing bacteria and archaea in temperate forest soils. Soil Biology and Biochemistry, 94, 169–172. https://doi.org/10.1016/j.soilbio.2015.11.015

20. **Nguyen, L. T., Schmidt, H. A., Von Haeseler, A., & Minh, B. Q. (2015).** IQ-TREE: a fast and effective stochastic algorithm for estimating maximum-likelihood phylogenies. Molecular biology and evolution, 32(1), 268-274.
21. **Oksanen J, Blanchet FG, Kindt R.** Vegan: community ecology package. R Package Ver. 2013;2:0–10.
22. **Ouyang, Y., Norton, J. M., & Stark, J. M. (2017).** Ammonium availability and temperature control contributions of ammonia oxidizing bacteria and archaea to nitrification in an agricultural soil. Soil Biology and Biochemistry, 113, 161-172.
23. **Rosen MJ, Callahan BJ, Fisher DS, Holmes SP. (2012).** Denoising PCR-amplified metagenome data. BMC Bioinformatics 13: 283.
24. **Rotthauwe, J. H., Witzel, K. P., & Liesack, W. (1997).** The ammonia monooxygenase structural gene amoA as a functional marker: molecular fine-scale analysis of natural ammonia-oxidizing populations. Applied and environmental microbiology, 63(12), 4704-4712.
25. **Sedlacek, C. J. (2020).** It takes a village: discovering and isolating the nitrifiers. Frontiers in Microbiology, 11. DOI:10.3389/fmicb.2020.01900.
26. **Shen, J. P., Zhang, L. M., Di, H. J., & He, J. Z. (2012).** A review of ammonia-oxidizing bacteria and archaea in Chinese soils. Frontiers in Microbiology, 3(AUG), 1–7. https://doi.org/10.3389/fmicb.2012.00296
27. **Siljanen, H. M. P., Alves, R. J. E., Ronkainen, J. G., Lamprecht, R. E., Bhattarai, H. R., Bagnoud, A., Marushchak, M. E., Martikainen, P. J., Schleper, C., & Biasi, C. (2019).** Archaeal nitrification is a key driver of high nitrous oxide emissions from arctic peatlands. Soil Biology and Biochemistry, 137, 107539. https://doi.org/10.1016/J.SOILBIO.2019.107539.
28. **Stempfhuber, B., Engel, M., Fischer, D., Neskovic-Prit, G., Wubet, T., Schöning, I., Gubry-Rangin, C., Kublik, S., Schloter-Hai, B., Rattei, T., Welzl, G., Nicol, G. W., Schrumpf, M., Buscot, F., Prosser, J. I., & Schloter, M. (2015).** pH as a Driver for Ammonia-Oxidizing Archaea in Forest Soils. Microbial Ecology, 69(4), 879–883. https://doi.org/10.1007/s00248-014-0548-5

29. **Taylor, D. L., Walters, W. A., Lennon, N. J., Bochicchio, J., Krohn, A., Caporaso, J. G., & Pennanen, T. (2016).** Accurate estimation of fungal diversity and abundance through improved lineage-specific primers optimized for Illumina amplicon sequencing. Applied and Environmental Microbiology, 82(24), 7217–7226.
30. **Tourna, M., Freitag, T. E., Nicol, G. W., & Prosser, J. I. (2008).** Growth, activity and temperature responses of ammonia-oxidizing archaea and bacteria in soil microcosms. Environmental Microbiology, 10(5), 1357-1364.
31. **Vitousek PM, Gosz JR, Grier CC, Melillo JM, Reiners WA. (1982).** A Comparative Analysis of Potential Nitrification and Nitrate Mobility in Forest Ecosystems. Ecological Monographs 52: 155–177.
32. **Zak, D. R., Host, G. E., & Pregitzer, K. S. (1989).** Regional variability in nitrogen mineralization, nitrification, and overstory biomass in northern Lower Michigan. Canadian Journal of Forest Research, 19(12), 1521–1526. https://doi.org/10.1139/x89-231.
33. **Zak, D. R., Pregitzer, K. S., & Host, G. E. (1986).** Landscape variation in nitrogen mineralization and nitrification. Canadian Journal of Forest Research, 16(6), 1258–1263. https://doi.org/10.1139/x86-223.